Experiments in Fluids 24 (1998) 431–446 © Springer-Verlag 1998

Expanding the applications of holographic interferometry to the quantitative visualization of oscillatory thermofluid processes using temperature as tracer

C. Herman, E. Kang, M. Wetzel

Abstract In this paper we discuss a novel application of holographic interferometry in the simultaneous quantitative visualization of high-speed, oscillatory flow and temperature fields in complex flow geometries. We consider cases of (i) self-sustained oscillatory flows with main flow imposed in grooved and communicating channels as well as (ii) oscillating thermofluid processes with zero mean velocity in a thermoacoustic refrigerator model. Examples showing unsteady temperature distributions obtained by real-time holographic interferometry combined with high-speed cinematography illustrate the possibilities of the approach introduced in the paper. Our study shows that temperature distributions accurately mirror flow structures in certain types of complex, unsteady flows, thus allowing, apart from the measurement of temperature profiles and heat transfer, also the measurement of oscillatory amplitudes, frequencies, wavelengths as well as the speed of propagation of traveling waves by applying digital image processing techniques. In the grooved and communicating channels it is possible to visualize the structure of the Tollmien–Schlichting waves through isotherms by using the infinite fringe field alignment of holographic interferometry. In the thermoacoustic refrigerator model, small amplitude temperature oscillations generated by the acoustic standing wave are visualized and measured. Image processing as well as data reduction procedures used in the analysis of these flow fields are discussed in the paper. Experimental data obtained by applying the techniques introduced in the paper show good agreement with theory and results of numerical simulations. Our study suggests that using temperature as tracer offers numerous advantages in the study of certain types of complex, unsteady flows.

List of symbols

a	evaluation constant in HI, $a=\lambda/l\,(n_\infty-1)$
D_h	hydraulic diameter of the grooved channel, $D_h=4lH/2(l+H)$, m
DR	drive ratio, $\mathrm{DR}\equiv P_A/p_m$
f	frequency, Hz
H	channel height (Fig. 1a), plate spacing in stack (Fig. 1b), m
L	periodicity length, m
l	spanwise dimension of the test section, m
n	refractive index
N	number of samples
p, P	pressure, Pa
$\bar{r}(\lambda)$	specific refractivity, m^3/kg
R	gas constant, $J/(kg\,K)$
Re	Reynolds number, $Re_g\equiv u_m D_h/\nu$, $Re_c\equiv\frac{3}{2}\,u_m H/\nu$
S	interference order
t	time, s
T	temperature, K
u	flow velocity, m/s
x	streamwise coordinate, m
x_c	stack center position, m
Δx	stack length, m
y	heightwise coordinate, m
z	spanwise coordinate, m

Greek letters

δ	small deviation from mean value
Δ	difference
γ	ratio, isobaric to isochoric specific heats
λ	wavelength, m
λ_{TS}	wavelength of Tollmien–Schlichting waves, m
ν	kinematic viscosity, m^2/s
ω	angular frequency, rad/s

Subscripts

A	amplitude
c	refers to communicating channels
corr	correction
crit	critical value
g	refers to grooved channel
i, j	count variables
m	mean value
meas	measured value
samp	sampling
th	theoretical
∞	reference state

Received: *7 January 1997*/*Accepted*: *18 September 1997*

C. Herman, E. Kang, M. Wetzel
Department of Mechanical Engineering
The John Hopkins University
3400 N. Charles St., Baltimore, MD 21218, USA

Correspondence to: C. Herman

This work is supported by the National Science Foundation Grant Number CTS-9310146 and by the Office of Naval Research.

1
Introduction

Conventional flow visualization techniques, such as the injection of tracers, allow the experimenter to gain mainly qualitative insight into flow structures. The injection of dyes or solid particles (such as ink or aluminum particles) into the liquid has been implemented in the study of self-sustained oscillatory flows in the past (Sobey 1982; Patera and Mikic 1986; Greiner 1991; Xi et al. 1995). The images obtained in this way provided information regarding the onset of oscillations, verified the presence of recirculation regions and wavy structures, and were suitable for a qualitative comparison and verification of predictions obtained by numerical simulation. However, these methods usually do not yield sufficiently accurate quantitative information on complex, unsteady flow structures. Conventional visualization techniques also require careful selection of tracer or dye material, to avoid buoyancy effects that can easily corrupt experimental data. Another disadvantage of dye and particle injection is the possible contamination of the test section of the experimental setup.

Measurement techniques used in quantitative studies of fluid flow include *field measurements*, such as holography, Particle Imaging Velocimetry (PIV), Holographic Particle Imaging Velocimetry (HPIV) and speckle photography, as well as local measurements obtained, for example, by hot wire anemometry or Laser Doppler Anemometry (LDA) (Herman et al. 1992). Field measurements allow the mapping of quantitative flow information in the region of interest, i.e. flow velocity distributions as continuous function of spatial coordinates at discrete instants of time. In recent years the field of quantitative flow visualization has been experiencing intensive growth, and the number of complex applications reported in the literature is increasing. *Local measurements* yield temporally continuous information at a specified spatial location during the time interval of interest. However, in the case of unsteady processes, these techniques are not suitable for mapping local velocities in the entire region of interest, since sensor information obtained subsequently at different locations during different experimental runs is difficult to correlate in order to reveal the spatio-temporal structures developing in the flow field.

In the present paper we introduce an alternative to the flow measurement techniques discussed above that allows, apart from physical insight, also the quantitative study of certain features of high-speed oscillatory thermofluid processes in complex two-dimensional geometries. Holographic Interferometry (to be abbreviated as HI in the text to follow) is frequently applied in engineering sciences in the visualization of refractive index fields, such as temperature, species concentration, as well as density in compressible flows. HI offers the usual advantages of optical measurement techniques; it is nonintrusive and it can provide high spatial and temporal resolutions. A number of quantitative studies of unsteady, particularly high-speed refractive index fields has been reported in the literature (such as heat transfer at the interface of condensing bubbles, Mayinger and Chen (1986); turbulence in an air stream with fluctuating temperature, Erbeck and Merzkirch (1988); temperature fields in a mixing vessel, Ostendorf and Mewes (1988); interaction between a shock wave and a turbulent boundary layer, Lanen et al. (1992); density fields in supersonic jets and convective flow, Söller et al. (1994) — to mention only a few…). In the aforementioned analyses refractive index data were obtained for individual images or image pairs recorded at specific instants of time, and information on the time dependence of characteristic flow features was not sought. The feasibility, potential and limitations of HI in the quantitative analysis of unsteady flow fields (in addition to the fairly common heat transfer measurements) through visualization of isotherms has not yet been investigated systematically, in spite of the fact that a certain amount of information on the flow structure is carried in the image of the temperature field. The objective of the present paper is to report results of such investigations and contribute to the filling of this void in the technical literature.

2
Physical situation

Oscillatory flows naturally occur in a variety of physical situations. In the past four decades numerous studies have addressed issues specific for *purely oscillatory* and *modulated flows* (oscillatory flow superimposed on a mean steady flow). Typical applications include enhancement of heat transfer and species transport, chemical species separation, flow control, flow velocity measurement equipment calibration and biomedical applications. Recent advances in the study of oscillatory flows were reviewed by Cooper et al. (1993). In the present paper we summarize our experience in the study of these flows accumulated during the past eight years while covering three research projects: the study of self-sustained oscillatory flows and the accompanying heat transfer in (i) grooved and (ii) communicating channels and the study of (iii) oscillatory flow and heat transfer in thermoacoustic refrigerators.

During the past three decades the development of compact heat transfer surfaces has been receiving much attention in the research community. It has been found that oscillation of the driving flow is a promising approach to heat transfer augmentation (Ghaddar et al. 1986a, b). Resonant heat transfer enhancement, a passive technique, is appropriate for systems with naturally occurring separated flows, such as the grooved and communicating channels shown in Fig. 1a. Grooved channels are typically encountered in electronic cooling applications and communicating channels represent a model of the rectangular plate fin, offset-fin and offset strip-fin flow passages of compact heat exchangers as well as heat sinks used in electronic packaging solutions. The enhanced surfaces we investigated involve the repeated formation and destruction of thin thermal boundary layers by interrupting the heat transfer surface in the streamwise direction, as illustrated schematically in Fig. 1a.

In addition to their practical significance, the two situations presented in Fig. 1a are examples of separated shear flows with complex interactions of separated vortices, free shear layers and wall bounded shear layers. In both channel geometries, two main flow regions, separated by a free shear layer, can be recognized: (i) the bulk flow in the main channel and (ii) the weak recirculating vortex flow in the groove or communicating region. In laminar, steady-state conditions there is virtually no exchange of fluid between these two regions. The results of Patera and Mikic (1986), Karniadakis et al. (1987), and

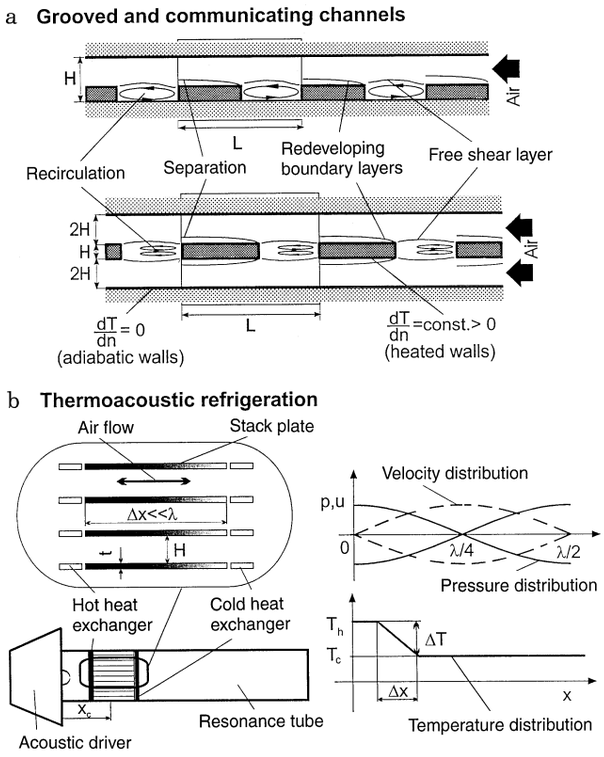

Fig. 1. **a** Schematic of channel geometries for investigation of self-sustained oscillatory flows and the physical situation in grooved and communicating channels; **b** schematic and basic operating principles of a thermoacoustic refrigerator. Velocity, pressure and temperature distributions along the resonance tube

Greiner et al. (1990) showed that self-sustained oscillations develop in such flow configurations at a relatively low Reynolds number in the transitional regime, and the interaction of separated flow with imposed unsteadiness leads to significant lateral convective motions, resulting in overall transport enhancement.

Our first experiments focusing on the investigation of heat transfer enhancement in communicating channels by visualizing high-speed, unsteady temperature fields and comparing these data with results of numerical simulations, indicated that the selected experimental technique, HI, can be applied successfully to study oscillatory heat transfer problems (Amon et al. 1992, 1993). The experimental visualization of Tollmien–Schlichting waves by using temperature as tracer was proven to be an effective method to gain quantitative insight into fast changing flow structures in our study. In this paper we focus on the measurement method used to study the characteristics of the flow fields rather than on results regarding heat transfer. The reader interested in the heat transfer aspect of these problems is referred to other publications (Amon et al. 1992, 1993; Farhanieh et al. 1993; Herman 1994). Since initial results regarding heat transfer enhancement were promising, the study of self-sustained oscillatory flows was later broadened to include grooved channels, and further information on heat transfer issues is available in the literature (Herman et al. 1997).

HI can also be applied to visualize time dependent temperature distributions in oscillating flows with zero mean velocity. A need for such measurements arose in the investigations of heat transfer in thermoacoustic refrigerators. Thermoacoustic refrigeration is a new, environmentally safe refrigeration technique that was developed during the past two decades (Wheatley et al. 1983; Swift 1988). The schematic of a thermoacoustic refrigerator is presented in Fig. 1b. The purpose of the acoustic driver is to generate an acoustic standing wave in the resonance tube. Thus, the working fluid in the resonance tube oscillates with zero mean velocity. The corresponding velocity and pressure distributions along the resonance tube are also displayed in Fig. 1b. Due to a thermal interaction between the oscillating working fluid and the densely spaced stack plates, a temperature gradient develops along the stack plates, that yields the temperature distribution shown in Fig. 1b. To exploit the transport of energy responsible for this temperature gradient for the purpose of refrigeration, heat exchangers are attached at both ends of the stack plates. The cold heat exchanger supplies the desired cooling load to the stack, while the hot heat exchanger rejects the pumped heat from the stack to the environment. For a more detailed discussion of thermoacoustic refrigeration the interested reader is referred to specialized literature (Wheatley et al. 1983; Swift 1988; Wetzel and Herman 1997a). One of the reasons why thermoacoustic refrigeration has not yet found commercial applications is the poor performance of the heat exchangers. As we will show in this paper, an appropriate tool to explore heat transfer at the edge of the stack plates and in the vicinity of the heat exchangers is HI combined with high-speed cinematography.

The aim of this paper is to advance holographic interferometry as an experimental technique that simultaneously renders quantitative flow and heat transfer data. We demonstrate that for studies similar to ours HI is superior to conventional flow visualization techniques, such as tracer methods or dye injection, since it can provide not only qualitative but also quantitative insight into certain types of unsteady flows. Several types of flows amenable for quantitative evaluation will be analyzed in the paper. We begin the discussion by introducing the experimental apparatus and technique. Next we present, based on the three case studies, numerous examples of how quantitative flow data can be extracted from interferometric visualization images. Data reduction procedures, image processing tools, experimental uncertainties as well as advantages and limitations of the method are explained, and questions requiring further study are addressed in the paper.

3
Experimental setup

3.1
Self-sustained oscillatory flows

Self-sustained oscillatory flows were studied in two specially designed wind tunnels that use air as working fluid. The blocks attached to the bottom of the grooved channel and the plates in the central plane of the communicating channels are heated electrically, and the thermal boundary condition on their surface is given by constant heat flux, as indicated in Fig. 1a.

The top and bottom plane walls of the test section are manufactured of low thermal conductivity material to maintain approximately adiabatic thermal boundary conditions. Details on the experimental setup and instrumentation are available elsewhere (Amon et al. 1992; Herman 1994; Herman et al. 1997).

In both channels, above a critical Reynolds number and at sufficient downstream distance, a periodically, fully developed flow regime is established. This region is of interest in visualization experiments, since the instantaneous velocity and temperature fields repeat periodically in space. Thus temperature fields are visualized in the region of the ninth heated block (there were 11 blocks in the test section), sufficiently far downstream to satisfy the periodicity requirement. This was verified through the heat transfer analysis presented elsewhere (Amon et al. 1992, 1993; Farhanieh et al. 1993; Herman 1994; Herman et al. 1997; Xi et al. 1995). The channel height to spanwise dimension aspect ratio is selected to ensure that the flow and temperature fields investigated by HI are two-dimensional.

3.2
Thermoacoustic refrigerator

To investigate temperature fields in the region of the stack and heat exchangers using HI, we built a thermoacoustic refrigerator model with a transparent stack region that allows the irradiation of the measurement volume with laser light. A schematic of the model is displayed in Fig. 11. Since our study of thermoacoustic refrigeration represents the first quantitative evaluation of temperatures measured with HI in an acoustic field, the primary design goal was to accommodate requirements imposed by HI. Therefore, we focused our attention on two stack plates and modeled the linear temperature distribution, shown in Fig. 1b, with heater foils. As we will demonstrate in Sect. 5.1.2, this modeling can be considered as using temperature as tracer to resolve small acoustic temperature oscillations.

In order to accommodate HI, some characteristic length scales of the thermoacoustic refrigerator, such as the plate spacing H, stack center position x_c, as well as stack length Δx had to be enlarged when compared to practical devices (Wetzel and Herman 1997b). These length scales are shown in Fig. 1b. For example, the selection of a suitable plate spacing for the thermoacoustic refrigerator model is a result of a compromise between mechanical constraints, such as manufacturing accuracy, stability and total dimensions of the setup, and optical constraints, determined by the spatial resolution of film material and possibilities of the lens system used for photographic recording. For the purpose of this study the plate spacing was chosen to be $H = 3$ mm. The cross section of the resonance tube is rectangular (157 mm $\times$ 63.5 mm) to yield a two-dimensional temperature distribution in the Cartesian coordinate system. For the interested reader we refer for a more detailed description of the model's design to the literature (Wetzel and Herman 1997b).

4
Experimental method

Holographic interferometry uses light as information carrier to provide qualitative and quantitative data on the investigated phenomenon. In convective heat transfer measurements the temperature fields in the thermal boundary layer above the heated surface and in the transparent working fluid are of interest. For more details about the technique, the reader is referred to the comprehensive literature on this topic (general information: Vest 1979; Mayinger 1994; specific information on the optical setup used in our studies: Amon et al. 1992; Herman 1994).

A standard *optical arrangement* for HI is presented in Fig. 2. The light source is a laser. We have used both a 25 mW Helium–Neon and a 1 W Argon-Ion laser in our experiments. The type and wavelength of the laser determine the choice of holographic and film materials for highest sensitivity, resolution and contrast, which is especially critical in high-speed applications. The laser beam is divided into a reference beam, RB, and an object beam, OB, by means of a, usually variable, semitransparent mirror (beam splitter), BS. Both beams are then expanded into parallel light bundles by a beam expander, BE, which consists of a microscope objective, a spatial filter and a collimating lens. The object beam passes through the test section, TS, with the phase object (representing the refractive index field to be related to temperature, concentration or density in the evaluation phase) and then falls on the holographic plate, H. The reference beam falls directly onto the holographic plate.

HI can be used to visualize and study high-speed, transient phenomena by using the *real-time method*, which is a single-exposure technique. The visualization is carried out in two steps. First, the reference state (usually with the fluid in the

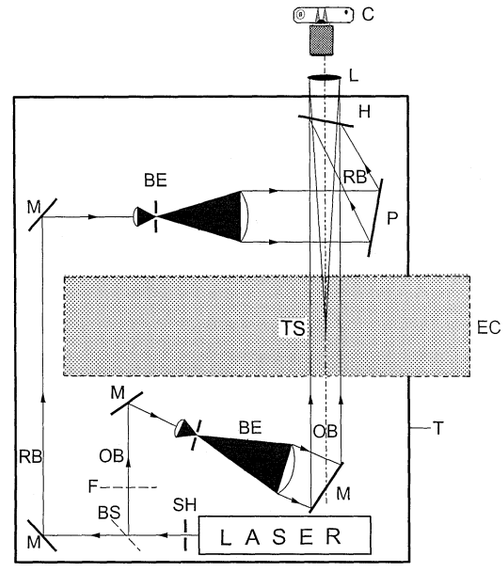

Fig. 2. Schematic of the optical setup for visualization of temperature fields used in the double exposure and real-time methods of holographic interferometry

measurement volume at ambient temperature) is recorded. Then the holographic plate is developed, bleached, dried and exactly repositioned into the plate holder. In the second step, the reference state of the object under investigation is reconstructed by illuminating the holographic plate with the reference beam. At the same time, the physical process is initiated, i.e. the blocks in the wind tunnel are heated or the thermoacoustic refrigerator is activated. Due to the heating, the refractive index of the fluid in the measurement volume changes, and, consequently, the object wave experiences a phase change on its way through the test section. The difference between the reference state recorded earlier and the new state of the fluid in the measurement volume is visualized in the form of an interference fringe pattern.

If the object wave at a later time during the measurement is identical to the original state for which the reference hologram was recorded, no interference fringes will appear. This state can be adjusted immediately before initiating the experiment, and the corresponding method of reconstruction is called the *infinite fringe field alignment*. The infinite fringe field alignment was used in all measurements reported in this paper. When the heat transfer process is initiated, the object wave becomes distorted, and behind the hologram the object and reference waves interact to form a macroscopic interference pattern. This we record with a high-speed camera with speeds of up to 10000 image frames per second. The interferometric fringes obtained using the infinite fringe field alignment correspond to isotherms, and are suitable, apart from the fairly common temperature measurments, also for the quantitative visualization of fluid flow phenomena, which will be demonstrated in this paper.

Another alignment of the optical equipment frequently used in interferometric measurements is the *finite fringe field alignment*. In this method a small tilt is applied to the mirror denoted by P in Fig. 2, that projects the reference beam onto the holographic plate. At ambient conditions this tilt will cause a parallel macroscopic fringe pattern to form. Our experience indicates that the finite fringe field alignment is less suitable for quantitative flow visualization, since the fringe patterns cannot be easily and intuitively related to the flow field. An example contrasting images obtained by the infinite and finite fringe field alignments will be discussed later in this paper, and is shown in Fig. 8.

In heat transfer measurements, that were the original and primary objective of our investigations, high spatial resolutions are required to analyze thin thermal boundary layers in the vicinity of the heated surface in forced convection. In order to achieve sufficient accuracy in heat transfer measurements, the interferometric images in our experiments were recorded on 16 mm high-speed film first, then scanned, digitized with resolutions up to 2700 dpi, and finally evaluated quantitatively using digital image processing techniques. The cost of video equipment suitable for these high-speed heat transfer measurements would have been prohibitive, since the resolution of images recorded by digital video cameras decreases with increasing recording speed. In flow visualization experiments the spatial resolution is less critical than in temperature measurements, since the fringes relevant for the characterization of flow phenomena in the main channel and recirculating regions are wider than in the thermal boundary layer.

5
Results

5.1
Temperature fields and flow oscillations

5.1.1
Self-sustained oscillatory flows

Although the physical situations in the grooved and communicating channels are similar, different approaches were used to quantify the flow. The shape of the individual fringe pattern for the three situations considered in the paper had a strong impact on the method selected for extraction of quantitative data, and we demonstrate through examples some of the approaches applied in the analysis.

The flow rate in the grooved and communicating channels was varied in the laminar, transitional and turbulent regimes. Flow velocities were verified by measuring velocity profiles at characteristic locations in the flow using hot wire anemometry as well as by using multiple rotameters with partially overlapping measurement ranges. Interferometric fringes in Figs. 3 and 4 represent isotherms, and the temperature difference corresponding to a pair of fringes is approximately 2.8 K in these experiments (Hauf and Grigull 1970; Herman et al. 1992). The direction of the bulk air flow is from right to left in all interferometric images. Typical steady-state temperature fields in the grooved (top) and communicating channels (bottom), visualized by HI, are presented in Fig. 3. At these low Reynolds numbers, the flow is laminar and stable. The flow structure in the main channels resembles the fully developed internal flow situation with parabolic velocity profiles, as shown numerically by Amon et al. (1992). In the steady-state situation the recirculating flow is confined to the groove or to the communicating region, and there is virtually no communication between the main channels and recirculating flows. In the main channels, isotherms are parallel to the plane walls with waviness of different amplitude and wavelength imposed to the basic fringe pattern at higher Reynolds numbers, as displayed in Fig. 4.

In the interferometric images we can recognize regions relevant for the thermal analysis, and they at the same time

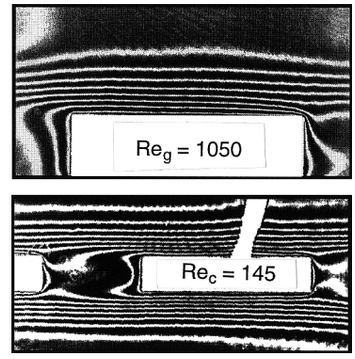

Fig. 3. Instantaneous temperature fields visualized by holographic interferometry in the form of isotherms in the grooved (top, $Re_g = 1050$) and communicating channels (bottom, $Re_c = 145$) for the steady-state situation

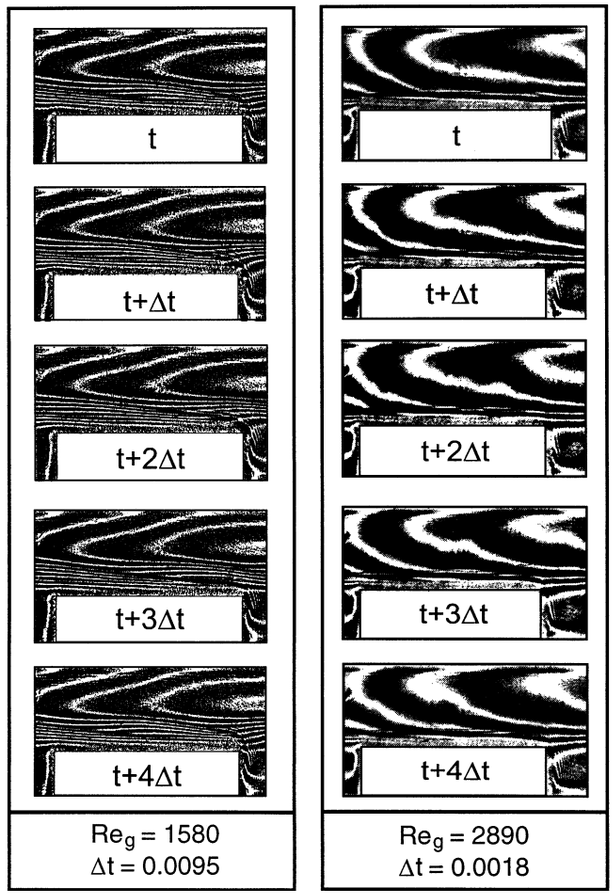

Fig. 4. Temperature fields in the grooved channel during a cycle of self-sustained oscillations at $Re_g = 1580$ and 2890

carry information on the oscillatory nature of the flow. The redevelopment of the thermal boundary layer — which corresponds to the region of redevelopment of the viscous boundary layer — along the top surface of the heated blocks in the grooved channel as well as along the two heated horizontal surfaces in the communicating channels is clearly visible in all images. In the redevelopment region isotherms are dense, illustrating a situation typical of high heat transfer coefficients. In the groove and communicating regions isotherms formed in the low speed recirculating flow are widely spaced, thus indicating smaller temperature gradients along the downstream heated vertical walls. The oscillatory effects and the wavy character of the flow in the main channel influence the thickness of the redeveloping thermal boundary layer along the plates by causing its successive expansion and compression.

Grooved channel

In the grooved channel the flow velocity is described by the Reynolds number defined as $Re_g \equiv u_m D_h / \nu$, where u_m is the mean air flow velocity averaged over a cross section at the channel inlet (corresponds to the dimensions of the cross section in the groove region). The critical Reynolds number for the onset of oscillations was found to be approximately $Re_{g,\,\mathrm{crit}} = 1320$, a flow rate significantly below the value characteristic for the onset of turbulence. The temperature oscillations that mirror the flow structure confirm the existence of a natural frequency in the investigated channel geometry. After the onset of oscillations, significant mixing between groove and bulk flows is initiated and it contributes to heat transfer enhancement. Typical histories of temperature fields corresponding to one period of oscillations at two representative Reynolds numbers, $Re_g = 1580$ and 2890, are shown in Fig. 4.

In the interferometric images shown in Fig. 4 two dominant oscillatory features were observed. The first feature is characterized by (i) *traveling waves of different wavelengths and amplitudes in the main channel*, visualized by moving isotherms, that are continuously being swept downstream. Typically, for $Re_g = 1580$, the waves are comprised of several isotherms assembled in a stack. The wave structures are characteristic of the Tollmien–Schlichting waves in the main channel, which are activated by the Kelvin–Helmholtz instabilities of the free shear layer spanning the groove, as discussed by Ghaddar et al. (1986a, b) and Amon et al. (1992). The critical Reynolds number for the onset of oscillations we found is somewhat lower than in the numerical and experimental studies of Ghaddar et al. (1986a, b) and Patera and Mikic (1986). This can be attributed to disturbances present in real flow situations as well as to the high sensitivity and temporal resolution of HI compared to dye injection or tracer methods used to identify the onset of oscillations in earlier visualization experiments.

The *speed of a traveling wave* can be determined by measuring the time it takes for the wave peak to traverse a known distance. The average propagation speed of the Tollmien–Schlichting waves was obtained by dividing the distance separating two characteristic channel points, for example the leading edge and the midpoint of the heated block shown in Fig. 5a, by the time elapsed. The time elapsed is found by counting the number of picture frames necessary for the center of the wave stack to traverse the distance between the two aforementioned points. The *frequency of traveling waves* is the inverse of the average wave period defined as the time required for two consecutive wave peaks to cross a fixed location during a given time interval.

The second characteristic oscillatory feature is observed at a location close to the leading edge of the heated block. The horizontal isotherm separating the main channel and groove regions remains relatively motionless for $Re_g = 530$. As the Reynolds number increases, the isotherm starts "whipping" up and down. Figure 5b shows a magnified view of the leading edge portion of the ninth heated block, and clearly illustrates the (ii) *whipping motion of the isotherm*, which is indicative of vertical velocity components. The heat transfer analysis of this problem, presented elsewhere (Herman et al. 1997), shows that these vertical velocity components are responsible for heat transfer enhancement along the upstream vertical wall of the block, as hot fluid from the groove is mixed with the colder main channel fluid.

For $Re_g = 1580$ the dominant frequency of the oscillatory whip was 29 Hz and corresponded well to the frequency of the traveling waves in the main channel, 26 Hz. At this Reynolds number two full waves, easily identified in Fig. 4 (left), spanned one geometric periodicity length. The data regarding wave

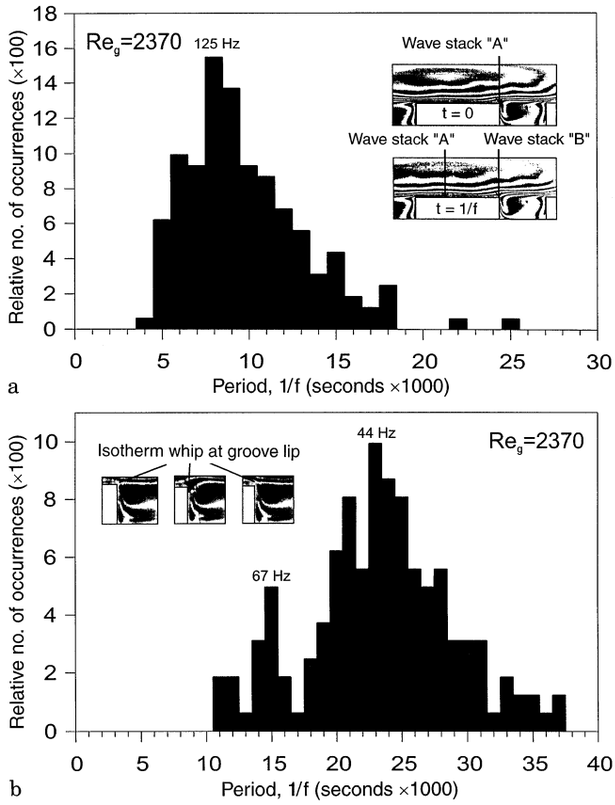

Fig. 5. Relative number of occurrences of recorded periods in the grooved channel for two different oscillatory events at $Re_g = 2370$. **a** The wave stack in the main channel passing over a selected landmark; **b** the oscillating isotherm upstream of the heated block. Interference patterns are included to illustrate the approaches selected to obtain the data presented in the diagrams

characteristics, such as wavelength, propagation speed and flow oscillations, obtained for two Reynolds numbers, $Re_g = 1580$ and 2370, and the number of images evaluated are summarized in Table 1. The correspondence of flow activities in the main channel and the groove region was apparent at $Re_g = 1580$, verified by the good agreement of the dominant frequencies shown in Table 1, and less so at $Re_g = 2370$.

The traveling waves were easily identified for the lower flow rate situations and were obviously much more difficult to discern for Re_g above 2000, as illustrated in Fig. 4. For $Re_g = 2370$ the method for data reduction had to be applied with more care, due to the high isotherm density near the block surface. Also, at this higher flow velocity, the isotherms near and above the main channel centerline widened, which created difficulties in identifying and tracking the propagating waves along the isotherms near the top surface of the block and thus left the tracking of the isotherms near and above the main channel centerline as the only alternative. The difficulty of quantifying flows in high-speed transitional and near-turbulent flow regimes is also characteristic of conventional dye injection techniques, where turbulence can in some cases render the method useless. Previous studies have shown (Xi et al. 1995) that at relatively low flow velocities, such as the

Table 1. Wavelength, oscillation frequencies and speeds of traveling waves in the grooved channel at $Re_g = 1580$ and 2370

Parameters	$Re_g = 1580$		$Re_g = 2370$	
	Main channel	Groove lip	Main channel	Groove lip
Waves/Period, L/λ_{TS}	1.85	N/A	2.94	N/A
Mean wave speed (m/s)	0.71	N/A	1.76	N/A
Dominant frequencies (Hz)	26	29	125	44, 67
Average period (s)	0.039	0.035	0.01	0.023
No. of periods analyzed	9	6	161	161
Total images sampled	350	208	1582	3754

situation for $Re_g = 1580$, the structure of the Tollmien–Schlichting waves is two-dimensional. However, at higher flow velocities three-dimensional effects may be present, and this issue requires attention in future studies.

Increasing the Reynolds number from 1580 to 2370 results in an increase of the frequency of the oscillatory whip and a much more pronounced increase of frequency of the propagating waves. On the average, at $Re_g = 2370$, the geometric periodicity contained three Tollmien-Schlichting waves. These three waves are also present at $Re_g = 2890$, but they are not as obvious or easy to recognize in Fig. 4 (right). For $Re_g = 2370$, the measured frequencies of the main channel wave activity and oscillating isotherm show more scatter than was the case for the lower Reynolds number. The dominant frequencies indicated in Table 1 have different definitions for $Re_g = 1580$ and 2370. For $Re_g = 1580$ the flow exhibits a more ordered behavior and the dominant frequency is the average of all the frequencies recorded. For the less regular flow situation at $Re_g = 2370$, the dominant frequency indicated in Table 1 corresponds to the peaks in the probability density charts shown in Fig. 5. The abscissa of Fig. 5 shows the range of oscillation periods which were recorded and the ordinate indicates the relative number of occurrences a certain period length was detected for the total of 161 periods analyzed. Raising the Reynolds number from 1580 to 2370 resulted in a probability density distribution that can be identified as a single (Fig. 5a) and bimodal (Fig. 5b) Gaussian distribution for the main channel wave and oscillatory isotherm activities, respectively.

The number of image frames that needs to be analyzed to determine frequencies and speeds of these two characteristic features depends primarily on the Reynolds number of the flow and on the appropriate recording speed for that particular Reynolds number. For low Re_g, when the flow is ordered and well behaved, several hundred images were analyzed. For Re_g greater than 2000, several thousand images were processed sequentially in order to obtain an acceptable sample for quantification of the disorderly flow behavior. These numbers are indicated in Table 1.

Communicating channels

The Reynolds number in the communicating channels is defined as $Re_c \equiv \frac{3}{2} u_m H/\nu$, where the characteristic length scale

H in this definition represents the half-height of the main channel. A temperature distribution obtained by HI for the steady-state regime is displayed in the bottom portion of Fig. 3. The critical Reynolds number for the onset of oscillations was experimentally determined to be around 200 and this result is in good agreement with data obtained numerically (Amon et al. 1992, 1993). At Reynolds numbers above the critical value for the onset of oscillations the vortices in the communicating region are unsettled and the steady state of the flow is disrupted. The vortex configuration becomes unstable, and vortices are ejected alternately to the top and bottom channels, thus inducing mixing between the vortex and bulk flows.

By analyzing sequences of interferometric images recorded by high-speed camera, different oscillatory regimes and varying oscillatory amplitudes were detected in the communicating channels. Two characteristic flow situations are illustrated schematically in Fig. 6, together with the corresponding temperature fields. One can notice the presence of a) four and b) three traveling waves over the double periodicity length in these images. As the flow structure in the communicating region is in agreement with the traveling wave structure in the main channels, the vortical structures in two successive communicating regions are either a) identical or b) antisymmetric, respectively. These observations for communicating channels were confirmed numerically by Amon et al. (1993).

The studies on communicating channels led to interesting discoveries regarding flow instabilities: different oscillatory regimes were detected and amplitudes of oscillations varied significantly at the same flow velocity and during the same experimental run. These phenomena, captured by visualizing temperature fields, are illustrated in Fig. 7, showing the history of temperature fields during one period of oscillations for two different oscillatory regimes developing at $Re_c = 493$. In the first set of interferometric images displayed in Fig. 7 (left) hardly any vortex activity can be observed in the communicating region, indicating reduced lateral mixing. The second sequence of interferometric images in Fig. 7 (right) was recorded during a time interval of the same length as the one corresponding to the sequence shown on the left hand side. The pattern of oscillations has changed, and the set of interferometric images displayed in Fig. 7 (right) shows intensive vortex activity in the communicating region, indicating that vortices ejected into the top and bottom channels improve lateral mixing. The intensity of waviness in the main channels does not change significantly. Similar effects were discovered by numerical simulation; details regarding the nature of this phenomenon and the

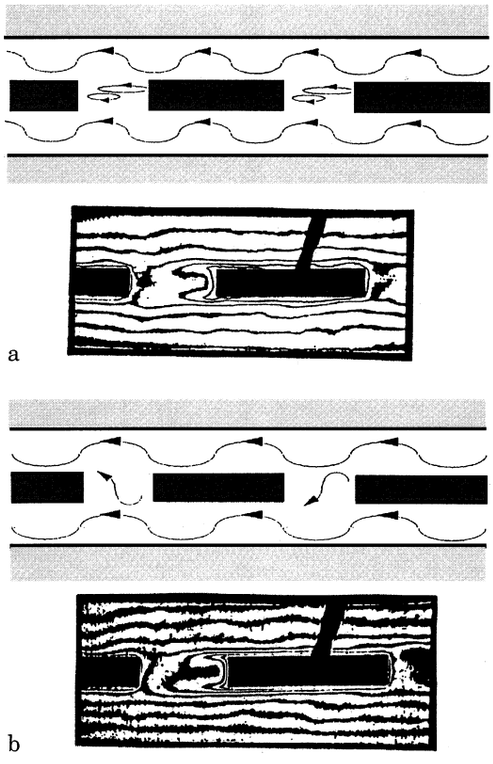

Fig. 6. Schematic of the physical situation in two geometric periodicity lengths along the communicating channels and corresponing visualized temperature fields. **a** Four waves, **b** three waves in the investigated region

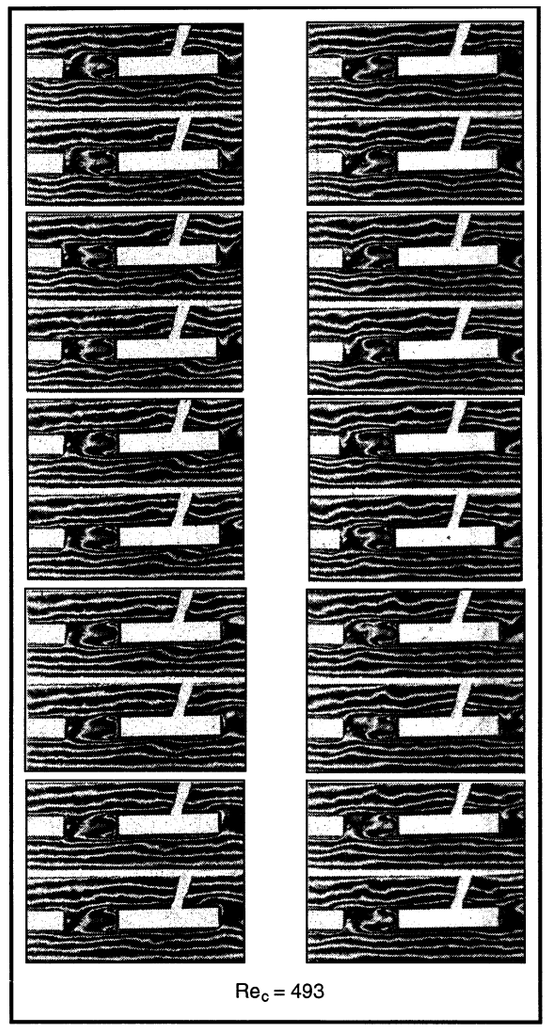

Fig. 7. Time history of temperature fields corresponding to different oscillatory regimes visualized by holographic interferometry in the communicating channels for $Re_c = 493$

quantitative study of oscillatory regimes are beyond the scope of the present paper and are presented elsewhere (Amon et al. 1992, 1993).

As discussed in Sect. 4, in order to demonstrate the advantages of using the infinite fringe field alignment in quantitative flow visualization, in Fig. 8 we compare the characteristic features of the fringe patterns developed along the first two heated plates in the communicating channels. These interferometric images were obtained using the finite fringe field alignment (top) and the infinite fringe field alignment (bottom). The initially imposed pattern for the finite fringe field alignment consisted of thin vertical fringes. The temperature distribution obtained by the infinite fringe field alignment allows good qualitative insight into the flow structures in the visualized region, as one can, for example, easily identify the redeveloping thermal and viscous boundary layers along the plates. Wide isotherms develop in the wake downstream of the plate. At $Re_c = 593$ the flow separates immediately downstream of the leading edge of the first block, and the location of the separation bubble is easy to detect in Fig. 8. Figure 8 clearly demonstrates the advantages of the infinite fringe field alignment in analyzing wave structures in the main channel flow. These cannot be identified in images obtained by the finite fringe field alignment.

In order to quantify the oscillatory flow in the vortex region of the communicating channels, we measured the locations of specific isotherms as a function of time for a sequence of up to 150 images for a series of Reynolds numbers using digital image processing. In Fig. 9a the measured positions of the isotherm extreme points in the vortex region, shown in the interferometric image in Fig. 9b, are plotted as a function of time for $Re_c = 593$. The oscillatory flow motion in Fig. 9a can be clearly recognized with the maximum for the upper vortex and the minimum for the lower vortex and vice versa. After applying the discrete Fourier transform to these data, the frequency spectrum of oscillations was obtained. The experimentally obtained Fourier spectrum at $Re_c = 593$ is presented in Fig. 9b, and the two carrying frequencies were determined to be 24.7 and 74.8 Hz. The evaluation of similar data for other Reynolds numbers showed that the spectrum also contains two dominant frequency peaks, and the values of the carrying frequencies increase with increasing Reynolds number. The results of these experiments are in good agreement with results of numerical simulations (Amon et al. 1993).

Both our experiments and results of numerical simulations (Amon et al. 1993) indicate that over a certain range of Reynolds numbers the three and four wavelength solutions illustrated in Fig. 6 can exist and alternate. The presence of two frequencies was observed over a wide range of Reynolds numbers, as shown in Fig. 10, where numerical, experimental as well as Tollmien–Schlichting frequencies are plotted over the Reynolds number in the range between $Re_c = 100$ and 600. For supercritical flows below a Reynolds number of approximately 200, the flow is time-periodic and exhibits a single fundamental frequency. In the regime of higher Reynolds numbers the flow is quasiperiodic and it mostly exhibits two dominant frequencies. In the low Reynolds number range the frequency values closely follow the three-wave Tollmien–Schlichting solution, whereas the increase in Reynolds number is marked by considerable deviation of the

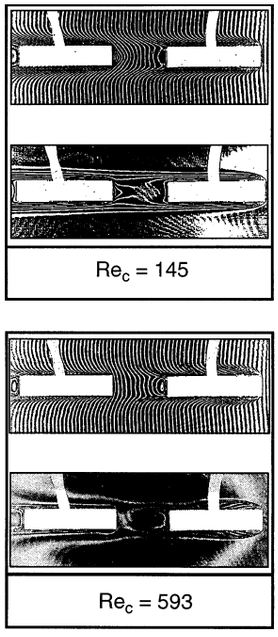

Fig. 8. Comparison of temperature fields developing around the first two heated plates in the communicating channels obtained using a finite fringe field (top) and the infinite fringe field alignment (bottom) of HI for $Re_c = 145$ and 593

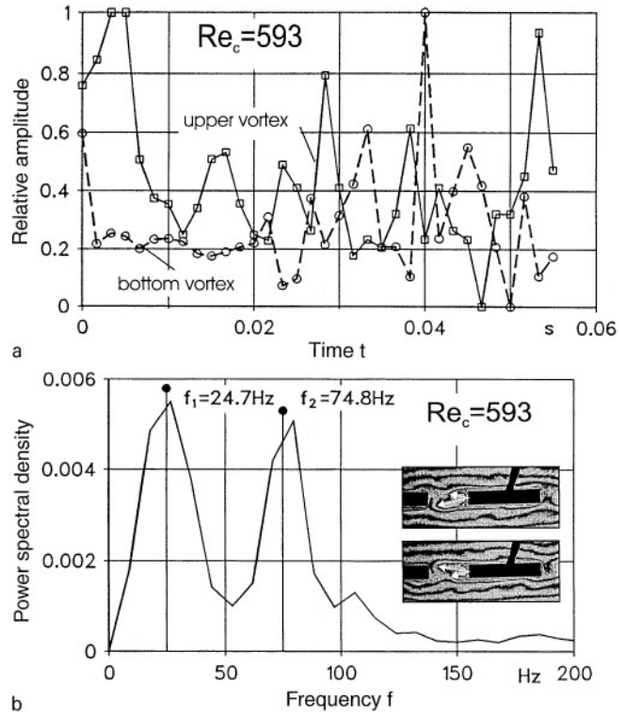

Fig. 9. **a** Amplitudes of isotherm extreme in the vortex region as function of time and the **b** Fourier power spectrum of oscillations at $Re_c = 593$. The interferometric images illustrate the data points used to characterize the oscillatory behavior of the flow

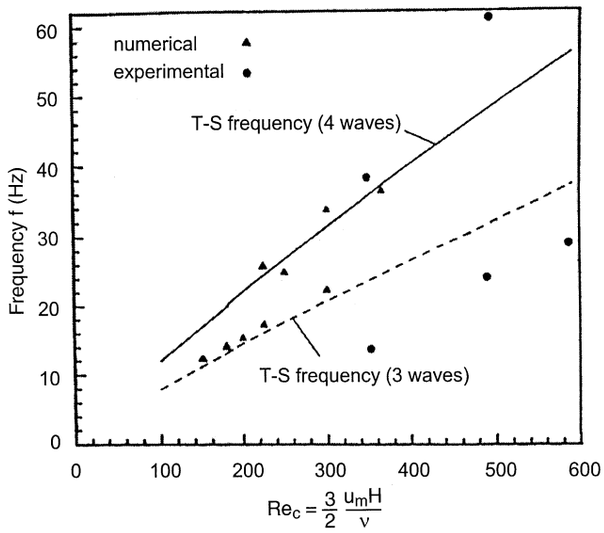

Fig. 10. Fundamental frequencies of self-sustained oscillations representing numerical results, experimental data and Tollmien–Schlichting solutions as a function of the Reynolds number (Amon et al. 1993). Tollmien–Schlichting solutions and numerical results are courtesy of Prof. C. Amon, Carnegie Mellon University

numerical and experimental frequency values from both four- and three-wave Tollmien–Schlichting solutions due to nonlinear effects.

5.1.2 Thermoacoustic refrigerator

As mentioned earlier, in thermoacoustics we are dealing with oscillating flow with zero mean velocity. The flow is acoustically driven and therefore causes the working fluid to adiabatically compress and expand. The successive compression and expansion cycles cause small, time dependent temperature fluctuations $\delta\, T(x, y, t)$ around the mean temperature $T_m(x, y)$, so that the temperature field can be represented as

$$T(x, y, t) = T_m(x, y) + \delta\, T(x, y, t) \tag{1}$$

The characterization of the temperature field by a linear combination of a time independent and a time dependent contribution also lays the foundation for the two step evaluation procedure when HI is applied to measure oscillating temperatures. In the first step, the mean temperature distribution $T_m(x, y)$, needed for an overall heat transfer analysis (Wetzel and Herman 1997b), is measured. Knowing the mean temperature distribution, the next step of determining the small temperature fluctuations $\delta\, T(x, y, t)$ can then be taken. An accurate measurement of these fluctuations is important for the analysis of the thermoacoustic effect, since it is the phasing between the oscillating velocity and temperature fluctuations that causes the transport of heat along the stack plates in a thermoacoustic refrigerator (Swift 1988).

For the measurement of the mean temperature distribution $T_m(x, y)$ it is necessary to identify one complete period of oscillations in a sequence of interferometric images. This is accomplished by tracing the movement of the interferometric fringes, as illustrated in Fig. 11. The presented set of interferometric images was recorded at a rate of 5000 picture frames per second, and the drive ratio DR was 1%. The drive ratio ($DR = P_A/p_m$) is an important flow parameter that characterizes the operating regime of a thermoacoustic refrigerator. The frequency of the acoustic oscillations was 337 Hz. Therefore, we captured 15 images corresponding to 15 time instants t_i of the oscillation's period. To reduce the amount of information presented to the reader and emphasize the differences between individual image frames, Fig. 11 shows 8 of these 15 images.

Following the motion of three fringes marked with 0, 0.5 and 1 through Fig. 11, we can illustrate how one period of oscillations was detected. As time progresses (Fig. 11a–d), the bright fringe numbered with 0 in Fig. 11a, breaks apart to form two fringes that move to the left and right along the Line Of Interest 2 (LOI 2), while the pair of bright fringes each numbered as 1 moves toward the center of the two stack plates, shown as gray bars in Fig. 11, along the LOI 1. During the same time sequence (Fig. 11a–d), the pair of dark fringes numbered as 0.5 moves along LOI 1 toward the center of the two stack plates until it merges (Fig. 11c) to form a single fringe. Then it breaks apart too, to form two fringes (Fig. 11d) moving in the direction perpendicular to the original direction along the LOI 2. Beyond this point (Fig. 11e–h) the interferometric fringes numbered with 0, 0.5 and 1 reverse their direction, until they have almost completed the cycle in Fig. 11 h.

To quantify the temperature field, a customized digital image processing algorithm described elsewhere (Wetzel and Herman 1997b) was applied, and the locations of the interference fringes for all 15 time instants of the oscillation's period were determined. To identify the locations of the fringes within the interferometric images, a coordinate system was defined with the origin at the lower left corner of the upper stack plate, as shown in Fig. 11a. Finally, temperatures were assigned to the interferometric fringes according to the evaluation formula by Hauf and Grigull (1970)

$$T(x, y, t) = \frac{T_\infty}{1 + a\ S(x, y, t)},$$

where

$$a = \frac{\lambda}{l(n_\infty - 1)} = \frac{2}{3}\,\frac{\lambda}{l}\,\frac{R\,T_\infty}{\bar{r}(\lambda)\,p_\infty} \tag{2}$$

Next, to obtain a spatially continuous temperture distribution for each time instant t_i, a least squares curve fit was applied to the discrete data points obtained in the evaluation process. Once these continuous temperature distributions were evaluated, we could take their average with respect to time over the 15 time instants t_i to determine the mean temperature distribution $T_m(x, y)$ of the oscillating temperature field $T(x, y, t)$.

Focusing now our attention on a fixed point in space, Point Of Interest (POI) in Fig. 11f, we can evaluate the small temperature fluctuations $\delta T(x, y, t)$. For this purpose, we plotted the temperature values $T_m + \delta T_{\text{meas}}$ measured at the POI for 48 interferometric images corresponding to 48 time instants t_i, as indicated in Fig. 12a. Then we subtracted the previously determined mean value $T_m(x, y)$ from these temperatures to be left with the time dependent contribution δT_{meas}, as

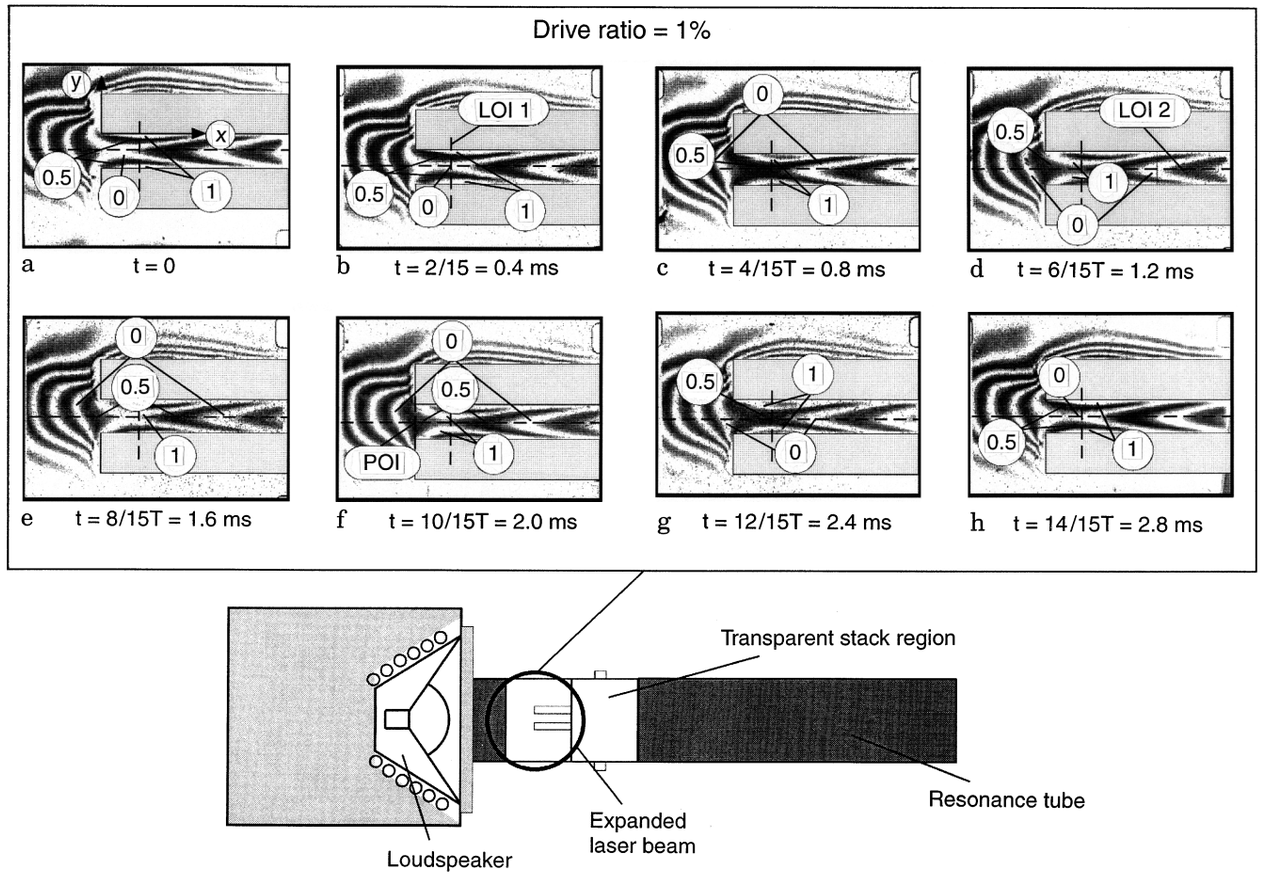

Fig. 11. Schematic of the thermoacoustic refrigerator model and interferometric images of the hot side of the stack region captured during one period of oscillations. These images were recorded at a rate of 5000 picture frames per second, the drive ratio was DR = 1%

shown in Fig. 12b. At this stage of the quantitative reconstruction the experimenter faces the problem that the changes in the refractive index depend not only on the small temperature fluctuations but also on the acoustic pressure variations. For such a case it was shown by Wetzel and Herman (1997b) that Eq. (2) cannot be applied to accurately determine the small temperature fluctuations δT. However, they also showed that the measured temperature fluctuations δT_{meas}, determined with Eq. (2), can be corrected to find δT as follows

$$\delta T\,(x, y, t) = \delta T_{\text{meas}}\,(x, y, t) + \delta T_{\text{corr}}\,(x, y, t)$$

where

$$\delta T_{\text{corr}} = \frac{\delta p}{p_m}\, T_m = \frac{P_A \cos\,(2\pi\, x/\lambda)}{p_m}\, \mathrm{e}^{\mathrm{i}\omega t} \tag{3}$$

to obtain an accurate value for the time dependent temperature field $T\,(x, y, t)$. The acoustic pressure fluctuations δp in Eq. (3) were obtained from information available on the acoustic standing wave, as indicated in Fig. 1b. The correction term δT_{corr} of Eq. (3) as well as the corrected temperature fluctuations δT for the POI, are also plotted in Fig. 12b. The interesting feature of the corrected temperature fluctuations δT is the fact that they are 180° out of phase with the data generated using Eq. (2). Consequently, Eq. (2) alone conveys a wrong image of the physical situation. In other words, while the working fluid appears to be in the compression stage of the acoustic cycle, in reality it is expanding.

Figure 12b also shows that the temperature fluctuation amplitude is of the order of 1 °C and such temperture variations are usually too small to be resolved with HI. Hauf and Grigull (1970) recommended at least 5 or more interference fringes in order to accurately evaluate the temperature field when using the infinite fringe field alignment. As discussed in previous sections, the finite fringe field alignment was found to be less suitable for the present study because of difficulties in the intuitive interpretation of the physical situation. Substituting the required number of fringes together with the appropriate reference state data ($T_\infty = 293$ K and $p_\infty = 101\,325$ Pa) into Eq. (2), we obtain a temperature difference, compared to the reference state, of at least 14 K. However, in this paper we have demonstrated that we were able to accurately resolve the much smaller acoustic temperature fluctuations $\delta T\,(x, y, t)$ because of the availability of the basic fringe pattern shown in Fig. 11. This pattern, instead of being generated by the small temperature fluctuations, was caused by a change of the reference state's temperature T_∞ to the mean temperature distribution $T_m\,(x, y)$ of the measurement state. The mean temperature distribution $T_m\,(x, y)$ develops as a result of two effects: (i) heating caused by resistive foils in the

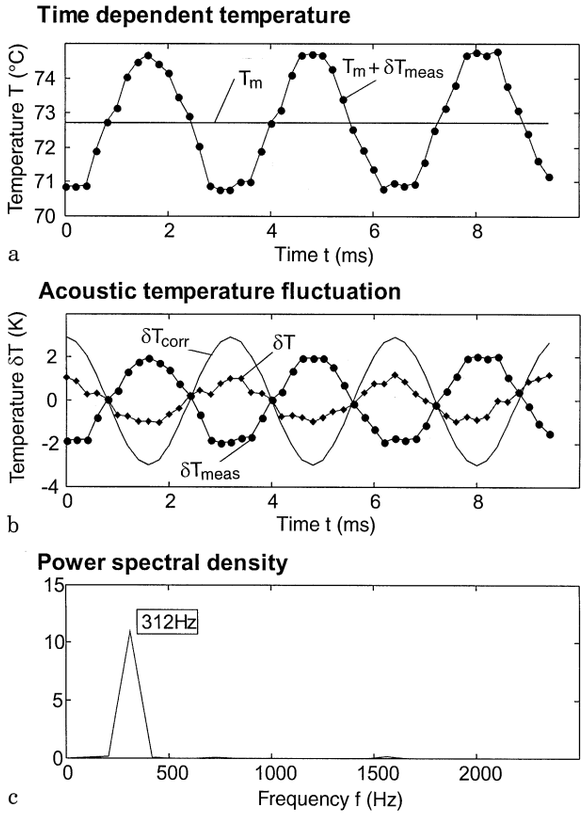

Fig. 12. **a** Temperature field evaluated with the conventional evaluation formula of HI at the POI; **b** small measured acoustic temperature fluctuations δT_{meas} (solid circles), their correction δT_{corr} (solid line) as well as the corrected data δT for the time dependent part of the temperature field (solid diamonds); **c** Power spectral density of the corrected temperature fluctuations

model's stack plates and (ii) the refractive index variations induced by the acoustic field. The contribution of the acoustic field is too weak to generate the number of interferometric fringes required for an accurate quantitative evaluation. The approach of using heater foils to generate the basic fringe pattern and thus imposing a mean temperature distribution $T_m(x, y)$ can be considered as adding a D.C. offset to the temperature field $T(x, y, t)$ during the experiment. After subtracting this D.C. offset from the temperature field during the quantitative evaluation, as illustrated in Fig. 12b, we are left with the small temperature fluctuations $\delta T(x, y, t)$. Thus the generation of the mean temperature distribution $T_m(x, y)$ with heater foils can be considered as "tagging" the working fluid with interference fringes. Then, by tracing these "tags", the temperature field $T(x, y, t)$ is determined. This discussion demonstrates how temperature can be used as tracer to visualize high-speed oscillating flow with the aim to resolve the small temperature fluctuations $\delta T(x, y, t)$, which introduces a new approach to accurately measure temperature fluctuations of the magnitude usually not amenable to quantification by HI.

Finally, in order to analyze the frequency characteristics of flow oscillations, we can apply signal processing tools such as a discrete Fast Fourier Transform (FFT) to obtain, for example, the power spectral density of the small temperature fluctuations. The power spectral density, displayed in Fig. 12c, shows one dominant frequency at 312 Hz, that corresponds to the carrying frequency of acoustic oscillations. The rather large discrepancy between the 312 Hz shown in Fig. 12c and the actual input frequency of 337 Hz can be attributed to the discretization in the frequency domain, and can easily be reduced by applying some of the measures described in Sect. 6. A more detailed discussion of this issue follows in Sect. 6 dealing with uncertainties of the measurements.

5.2 Digital image processing and measurement of interferometric fringe patterns

Interferograms contain spatially continuous 2D information on the field variable, temperature, at discrete instants of time, coded as irradiance distribution in the form of fringes. Having the amount of information contained in a single interferogram in mind, the extraction of quantitative data has presented a serious problem in the past and limited the applications of interferometry. This is especially true for high-speed, transient measurements, such as those reported in our paper, when several hundred or thousand images had to be analyzed in order to quantitatively characterize a single state. In this discussion we focus on the analysis of unsteady flow features rather than on temperture measurements that have been thoroughly covered in the literature (Vest 1979; Mayinger 1994).

The time history of an investigated feature is obtained by first identifying the feature in a sequence of interferograms, and then analyzing and measuring its change by comparing successive interferograms from this sequence. An example of this approach was given in Sect. 5.1.2 which dealt with the quantification of temperture oscillations at the POI in the stack region of the thermoacoustic refrigerator. The evaluation problem shows some similarities to the measurement of flow velocities using PIV: in PIV the displacement of a particle between two exposures (only) is measured to determine the local flow velocity. In HI the data reduction problem is more complex: in the analysis of transient phenomena, the problem of simultaneous visualization and quantitative comparison of multiple images, captured at different instants of time on different image frames, is added to the original data reduction and fringe analysis issues. In addition to this, the shape of the features to be compared can be quite complex in HI as opposed to the relatively simple particle shapes in PIV. The complexity of this image analysis problem calls for new solutions in the evaluation process.

We used a commercially available software environment, Bioscan Optimas Version 4.02, as basis for the development of application specific software. The first step of the application specific algorithm is to determine the position of the walls and the heated plates in the interferometric image. Based on the wall positions, a suitable coordinate system is defined, and the lines corresponding to irradiance minima and maxima are traced along each isotherm using a semi-automatic fringe tracing algorithm provided by Optimas. In this way data compacting is achieved by binarization; the gray level image is reduced to two intensity levels only. The data compacting

allows for easier analysis of the image by eliminating unnecessary details; it also increases processing speed and reduces memory requirements. The binary information is then stored in the form of an overlay on hard disk for further processing. The described image analysis and isotherm tracing procedure is repeated for the desired number of images.

In the following evaluation step, several of these overlays (usually not more than four to avoid loss of detail in the overcrowded picture) are superimposed, to observe the change of the transient process during the investigated time interval within a single image frame. Three superimposed overlays, obtained in the analysis of flow oscillations in the communicating channels, are shown in Fig. 13a. Color coding can be used to help distinguish between the superimposed overlays. Particular events and features can then be selected in such an image: markers are set to trace the motion of a characteristic point (for example, the points P1 and P2 in Fig. 13a denote wave minima moving in the flow direction in the upper and lower channels, respectively) between the individual exposures, as indicated in Fig. 13a. The coordinates of the marked points are exported to external files and can be subjected to further evaluation. Due to the complexity of the analyzed images, at this stage of the evaluation the markers are set manually, as judgment of the experimenter in identifying the characteristic features in a set of images is essential. For the investigated physical situation the described approach yielded satisfactory accuracy. Fully automated data processing would not be possible without the development of sophisticated image processing algorithms, which itself is a very time consuming process. The described evaluation procedure can easily be modified to accommodate different channel geometries and physical situations.

When evaluating the oscillating temperature fields in the thermoacoustic refrigerator model, we employed the template displayed in Fig. 13b. This template contained information on the location of the edges of the stack plates, the image specific coordinate system and the LOIs along which the interference orders were detected. As can be seen in Fig. 13b, we generated horizontal as well as vertical LOIs. The reason for this is that, for accurate quantitative evaluation, it is always favorable to select the LOIs to be perpendicular to the interferometric fringes. Thus, the horizontal LOIs were used to quantify the region outside the stack, while the vertical LOIs were used to evaluate the region between the two stack plates.

In order to analyze a sequence of images, this template is fit into each interferometric image, as shown in Fig. 13b. The number of data points specified in the evaluation process depends on the number of intersection points between LOIs and interference fringes. In case the experimenter is interested in higher spatial resolutions, the algorithm can easily be modified by adding more LOIs. However, we should note that the total number of LOIs is always a compromise between the required resolution and the time and effort needed to evaluate a sequence of interferometric images.

Once the spatial locations of the discrete data points have been acquired for each image, interpolation algorithms are applied to obtain continuos functions that describe the measured spatial temperature distribution for each interferogram. From these spatial temperture distributions it is then possible to evaluate the time dependent contribution to the temperture field as described in Sect. 5.1.2.

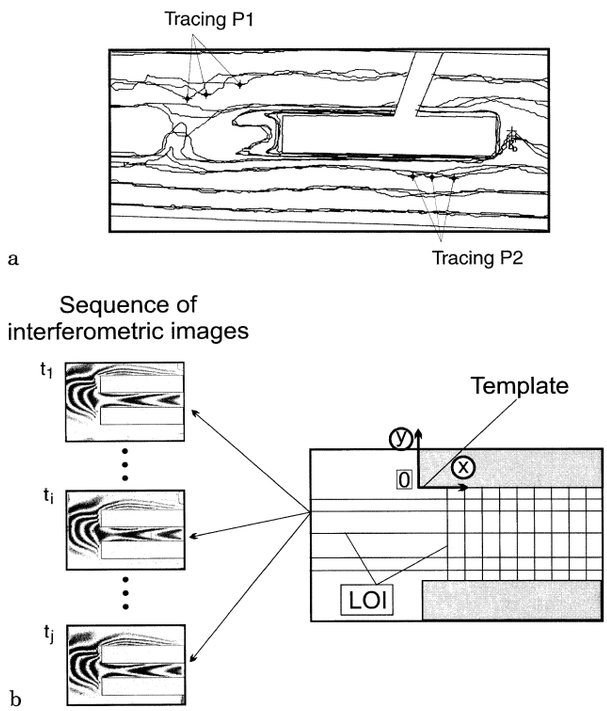

Fig. 13. a Three superimposed overlays obtained in the quantitative evaluation of an interferogram sequence. Points P1 and P2 trace the propagation of two minima of the Tollmien–Schlichting waves in the top and bottom channels, respectively; **b** template used in the evaluation of temperature distributions in a sequence of interferograms in the study of the thermoacoustic effect

6
Experimental uncertainties

Uncertainties in the experimental data are introduced by spatial and temporal discretization. It should be emphasized that using conventional film material to record interferograms allows us to achieve extremely high spatial resolutions, which is not the case when using expensive high-speed video cameras. The spatial resolution remains high after the scanning process (approximately 1300×760 pixels or 2100×1200 pixels in our applications, depending on the film scanner used). Focusing on portions of the interferometric image allows the experimenter to further increase spatial resolution.

6.1
Measurement of wavelengths and frequencies in the grooved channel

In the study of wave structures in the grooved channel, quantitative data obtained by analyzing high-speed film sequences is subject to uncertainties due to the subjective judgment of the experimenter. This uncertainty strongly depends on the individual experimental case that determines the isotherm pattern, and is a function of isotherm thickness, recording speed, and the shape of the Tollmien–Schlichting waves. Increasing the recording speed improves the temporal

resolution of the measurements and results in a smoother probability distribution for data similar to those presented in Fig. 5. The wave contour plays a potentially significant role in the uncertainty, as a flat wave makes the identification of the wave peak more difficult.

The abscissa of the probability distributions in Fig. 5 indicates the period of oscillations of two different oscillatory events: a) the propagation of the wave stack in the main channel and b) the oscillating isotherm along the free shear layer just upstream of the heated block. The temporal resolution defining the length of the period, $\Delta t = 0.001$ s, is determined by the camera's recording speed of 1000 picture frames per second. The measurement uncertainty for the oscillatory periods, a function of the manufacturer's specification for the high-speed camera, is $\pm 6\%$.

For $Re_g = 1580$, the standard deviations for the relative number of occurrences of the measured periods of the main channel waves and oscillating isotherm activities are 4.2% and 12.5%, respectively. The statistical characterization shows that these oscillatory activities, expressed through the relative number of occurrences of the oscillation periods, form a narrow band around the mean values listed in Table 1. The corresponding frequencies listed in Table 1 are: (i) 26 Hz for the main channel waves and (ii) 29 Hz for oscillations at the groove lip. At $Re_g = 2370$, the standard deviation for the relative number of occurrences of measured periods for the main channel waves and oscillating isotherm activities upstream of the block rises to 34.4% and 24.1%, respectively. This verifies the less orderly nature of the flow, and in certain cases suggests the existence of multiple dominant modes. In Fig. 5a, the distribution of recorded periods of the main channel waves is wide, with a single peak at 125 Hz. Figure 5b illustrates that the isotherm oscillations upstream of the heated block can be characterized by a bimodal distribution with dominant frequencies at 44 and 67 Hz.

6.2
Frequency measurements using the discrete FFT

For the Fourier analysis applied to the signals presented in Figs. 9a and 12b, the two well known requirements for the application of the discrete FFT have to be fulfilled: (i) the Nyquist criterion has to be satisfied and (ii) a high enough spectral resolution has to be achieved in the frequency domain. The Nyquist theorem states that the highest frequency that can be detected by the discrete FFT corresponds to half the sampling frequency f_{samp}, which in our experiments represents the frame rate of the high-speed camera. The time signals of Figs. 9a and 12b were sampled at 1200 and 5000 Hz, respectively. Thus, the highest frequencies that could be detected were 600 and 2500 Hz. Both these frequencies are an order of magnitude higher than values typical for the investigated physical phenomena, as can be seen from the power spectral densities in Figs. 9b and 12c.

The spectral resolution in the frequency domain depends on the sampling frequency f_{samp} as well as on the number of samples N acquired, and can be calculated as

$$\Delta f = \frac{f_{\text{samp}}}{N} \tag{4}$$

In the case of HI the number of samples N corresponds to the number of interferometric images evaluated in a sequence. Since the evaluation of the interferometric images is quite tedious, the spectral resolution is always a result of a compromise between the time and effort needed to obtain an acceptable number of samples and the desired accuracy.

For the signal shown in Fig. 9b, 136 interferometric images were evaluated. Together with a sampling rate of 1200 Hz, these values result in a spectral resolution in the frequency domain of $\Delta f = 8.8$ Hz. This resolution is high enough to clearly distinguish between the two dominant frequencies of 24.7 and 74.8 Hz. The same argument holds for the acoustic temperature fluctuations shown in Fig. 12b. For the Fourier transform of this signal we used 48 samples, which results in a spectral resolution of $\Delta f = 104$ Hz. Therefore, the closest frequency to the driving frequency of 337 Hz that we can resolve is 312 Hz, which explains the discrepancy mentioned in Sect. 5.1.2. This spectral resolution is sufficient to detect the presence of higher harmonics in the temperature fluctuations, which was one of the concerns when conducting these experiments. In both situations the spectral resolution can be easily enhanced by increasing the number of samples N, as dictated by the required accuracy.

6.3
Measurement of temperature fluctuations

To evaluate the uncertainties in the measurements of the small acoustic temperature fluctuations presented in Fig. 12b, we compare the corrected temperature data δT, determined at the POI, to the following theoretical model (Swift 1988)

$$\delta T_{th}(t_i) = \frac{\gamma - 1}{\gamma} \frac{P_A \cos(2\pi\ x/\lambda)}{p_m} T_m\, \mathrm{e}^{\mathrm{i}\omega t_i}. \tag{5}$$

From the theoretical data $\delta T_{th}(t_i)$ and the corrected data $\delta T(t_i)$, we can calculate the temperature difference $\Delta T_{\text{diff}}(t_i) = \delta T_{th}(t_i) - \delta T(t_i)$ for each of the 48 time instants t_i shown in Fig. 12b, and in the ideal case this difference should be zero. The standard deviation of this temperature difference from zero was found to be 0.2 K. From the standard deviation we calculated the uncertainty to be ± 0.1 K, with a confidence level of 99%.

7
Conclusions and outlook

The results of the experiments reported in this paper demonstrate that HI, apart from the measurement of unsteady temperature distributions and local heat transfer, also allows the quantitative study of flow characteristics for certain classes of oscillatory flows coupled with heat transfer, and it can be recommended in situations when quantitative local velocity data are not required. We can conclude that through visualization of temperature fields we can indirectly study flow instabilities and resonant modes, as well as measure wavelength, propagation speed and frequency of traveling waves. HI allows the visual identification of separated flow regions, and provides limited amount of detail regarding the recirculation region. However, it should also be pointed out that the method does not replace the widely accepted, nonintrusive velocity measurement techniques, such as LDA or

PIV, rather it complements them. Local velocity measurements with LDA are complemented by HI, that provides field information and thus allows better physical insight into the process. Real-time HI, the method applied in our experiments, enables the analysis of longer time intervals than covered by multi pulse lasers used in PIV or HPIV.

The advantage of the approach introduced in the paper over "classical" visualization methods (such as the use of tracers that allows qualitative insight only) is that quantitative information on the structure of flow and temperture fields as well as heat transfer is obtained simultaneously, using the same experimental setup and during the same experimental run, thus yielding consistent flow and heat transfer data. This feature makes the technique particularly attractive for applications such as the development of flow control strategies leading to heat transfer enhancement. Using temperture as tracer offers the additional advantage that a quantitative analysis of high-speed thermofluid processes becomes possible, since optical measurement techiques are nonintrusive, and, due to the high speed of light, have virtually no inertia. In the study of complex flow situations and flow instabilities, the investigated process can be very sensitive to disturbances, and the injection of dye or tracer particles can interfere with the flow, causing it to switch to another oscillatory regime due to perturbations. With HI, the contamination of the test section by tracers is avoided, thus allowing longer experimental runs and analyses of different steady states and transients during a single experimental run.

Whenever possible, the results presented in our paper were compared with data obtained using other approaches and reported by different authors. The good quantitative and qualitative agreement with data obtained in numerical simulation experiments and by theoretical predictions, as reported by Amon et al. (1992, 1993), proves the feasibility of our experimental approach. A more precise quantitative verification of the accuracy of reported flow parameters would require additional measurement data obtained by LDA or PIV, and it is expected that such data will become available in the future. The comparison of experimental results obtained in the thermoacoustic refrigerator study with results of numerical simulations (Worlikar and Knio 1996) shows good qualitative agreement. A quantitative comparison of experimental and numerical data is currently underway.

All applications discussed in the paper imply averaging in the spanwise dimension (along the light beam), and thus the experimental setup is designed to represent a simplified 2D model of the process. In the present form, HI is suitable for analyzing flows at low and intermediate flow velocities. As our results indicate, flow oscillations were easy to quantify at moderate flow velocities, such as the situation in the grooved channel at $Re_g = 1580$. At transitional Reynolds numbers ($Re_g = 2370$) the waves were much more difficult to discern, and a large number of images had to be analyzed to quantify the oscillatory features. This property of the measurement technique can partially be attributed to the spanwise averaging, and it underlines the limitations of the method in studying inherently three-dimensional flows near the onset of turbulence.

The effort involved in the study of high-speed, unsteady flows in the measurement phase and the extraction of quantitative information from the obtained images is significant. When analyzing oscillatory flows, the required recording frequencies are usually at least one order of magnitude higher than the frequency of the physical process. Due to the high sampling rates, thousands of images are generated within seconds, and these images are then successively processed to extract the required quantitative information. Algorithms for a completely automated analysis of images recorded by holography, PIV and HPIV are available. Algorithms that allow an automated analysis of images generated by HI have been described in the literature, however, at this point of time the issue has not yet been adequately resolved. This is especially true for unsteady processes.

The extent to which our methodology, developed for the study of oscillatory flows, can be generalized to analyze non-oscillatory unsteady flows, is an important question requiring systematic study. Another possibility of expanding the applications of HI would include artificially generating temperature differences at strategic locations in the flow channel to visualize flow features of interest, similarly to the method applied in the investigation of the thermoacoustic effect. In the quantitative interpretation of visualization images obtained in this way, buoyancy effects can influence the results at low flow velocities, thus the role of mixed convection has to be quantified. As shown in previous studies reviewed by Herman et al. (1992), the change of the refractive index can also be related to concentration changes, which would offer the option to use concentration as tracer in visualization experiments, in a similar fashion as temperature discussed in the present paper.

References

Amon CH; Majumdar D; Herman CV; Mayinger F; Mikic BB; Sekulic DP (1992) Numerical and experimental studies of self-sustained oscillatory flows in communicating channels. Int J Heat Mass Transfer 35: 3115–3129

Amon CH; Majumdar D; Herman CV; Mikic BB (1993) Fast evolving transport phenomena in self-sustained communicating-channels flows. Winter Annual Meeting of ASME, New Orleans, FED-Vol. 172, Eds. B. Khalighi et al., 351–358

Cooper WL; Yang KT; Nee VW (1993) Fluid mechanics of oscillatory and modulated flows and associated applications in heat and mass transfer — A review. J Energy Heat Mass Transfer 15: 1–19

Erbeck R; Merzkirch W (1988) Speckle photographic measurement of turbulence in an air stream with fluctuating temperature. Exp Fluids 6: 89–93

Farhanieh B; Herman C; Sunden B (1993) Numerical and experimental analysis of laminar fluid flow and forced convection heat transfer in a grooved duct. Int J Heat Mass Transfer 36: 1609–1617

Ghaddar NK; Korczak KZ; Mikic BB; Patera AT (1986a) Numerical investigation of incompressible flow in grooved channels. Part 1. Stability and self-sustained oscillations. J Fluid Mech 163: 99–127

Ghaddar NK; Magen M; Mikic BB; Patera AT (1986b) Numerical investigation of incompressible flow in grooved channels. Part 2. Resonance and oscillatory heat transfer enhancement. J Fluid Mech 168: 541–567

Greiner M; Chen RF; Wirtz RA (1990) Heat transfer augmentation through wall-shape-induced flow destabilization. J Heat Transfer 112: 336–341

Greiner M (1991) An experimental investigation of resonant heat transfer enhancement in grooved channels. Int J Heat Mass Transfer 34: 1383–1391

Hauf W; Grigull U (1970) Optical methods in heat transfer. In: Advances in Heat Transfer, Vol. 6, Academic Press, New York

Herman CV; Mewes D; Mayinger F (1992) Optical techniques in transport phenomena. Advances in Transport Processes VIII, Editors A.S. Mujumdar, R.A. Mashelkar, Elsevier Science Publishers, Amsterdam and New York, 1–58

Herman C (1994) Experimental visualization of temperature fields and measurement of heat transfer enhancement in electronic system models. Cooling of Electronic Systems, S. Kakac, H. Yuncu and K. Hijikata, Eds., NATO ASI Series, Vol. 258, Kluwer Academic Publishers, Dodrecht, 313–337

Herman C; Kang E; Vorreiter J (1997) Experimental visualization of temperature fields and study of heat transfer enhancement in oscillatory flow in a grooved channel. Accepted for publication in Int J Heat Mass Transfer

Karniadakis GE; Mikic BB; Patera AT (1987) Heat transfer enhancement by flow destabilization: application to the cooling of chips. Proc Int Symposium on Cooling Technology for Electronic Equipment, 587–610

Lanen TAWM; Bakker PG; Bryanston-Cross PJ (1992) Digital holographic interferometry in high-speed flow research. Exp Fluids 13: 56–62

Mayinger F Editor (1994) Optical measurements — Techniques and applications. Springer, Berlin

Mayinger F; Chen YM (1986) Heat transfer at the phase interface of condensing bubbles. Proc 8 Int Heat Transfer Conf, San Francisco, 1913–1918

Ostendrof W; Mewes D (1988) Measurement of temperture fields in mixing vessels using optical tomography. Chem Eng Technol 11: 148–155

Patera AT; Mikic BB (1986) Exploiting hydrodynamic instabilities. resonant heat transfer enhancement. Int J Heat Mass Transfer 29: 1127–1138

Sobey IJ (1982) Oscillatory flows at intermediate Strouhal number in asymmetric flows. J Fluid Mech 125: 359–373

Söller C; Wenskus R; Middendorf P; Meier GEA; Obermeier F (1994) Interferometric tomography for flow visualization of density fields in supersonic jets and convective flow. Appl Opt 33: 2921–2932

Swift GW (1988) Thermoacoustic Engines. J Acoust Soc Am 84: 1145–1180

Vest CM (1979) Holographic interferometry. Wiley, New York

Wheatley JC; Hofler T; Swift GW; Migliori A (1983) An intrinsically irreversible thermoacoustic heat engine. J. Acoust Soc Am 74: 153–170

Wetzel M; Herman C (1997a) Design optimization of thermoacoustic refrigerators. Int J Refrig 20: 3–21

Wetzel M; Herman C (1997b) Limitations of temperature measurements with holographic interferometry in the presence of pressure variations. Accepted for publication in Experimental Thermal and Fluid Science, in print

Worlikar AS; Knio OM (1996) Numerical simulation of a thermoacoustic refrigerator, I Unsteady adiabatic flow around the stack. J Compu Phy 127: 424–451

Xi GN; Hagiwara Y; Suzuki K (1995) Flow instability and augmented heat transfer of fin arrays. J Enhanced Heat Transfer 2: 23–32